J. Fluid Mech. (2006), *vol.* 569, *pp.* 249–258. © 2006 Cambridge University Press
doi:10.1017/S0022112006003016 Printed in the United Kingdom

Weakly nonlinear internal gravity wavepackets

By BRUCE R. SUTHERLAND

Department of Mathematical and Statistical Sciences, University of Alberta, Edmonton, AB, Canada T6G 2G1

(Received 3 July 2006 and in revised form 16 September 2006)

Horizontally periodic, vertically localized internal wavepackets evolve nonlinearly due only to interactions between the waves and their wave-induced mean flow. The corresponding weakly nonlinear equation that describes the evolution of the amplitude envelope before the onset of parametric subharmonic instability is examined. The results are compared with fully nonlinear numerical simulations and are shown to lie in excellent agreement for over 15 buoyancy periods. Analysis of the equation shows that the evolution is modulationally unstable if the wave frequency exceeds that of waves with the fastest vertical group speed and if the amplitude is sufficiently large. Waves that move close to the fastest vertical group speed are unstable even if their relative amplitude is a tiny fraction of the inverse relative vertical extent of the wavepacket. At late times in the evolution of an unstable wavepacket third-order dispersion terms become non-negligible and act in conjunction with weakly nonlinear effects to retard the vertical advance of the wavepacket as a whole.

1. Introduction

Internal waves move through a continuously stratified fluid vertically transporting energy and momentum, exerting drag and turbulently mixing where they break. The behaviour of small-amplitude waves is well-established, and some qualitatively different aspects of finite-amplitude waves have been revealed through laboratory experiments, analytic theories and fully nonlinear numerical simulations.

For example, monochromatic waves are unstable to parametric subharmonic instability (Klostermeyer 1991; Lombard & Riley 1996; Benielli & Sommeria 1996; Koudella & Staquet 2006). Such waves interact with themselves, transferring energy to longer time-scale, shorter spatial-scale waves. Wavepackets that are horizontally periodic but vertically localized additionally exhibit a phenomenon known as 'self-acceleration' (Fritts & Dunkerton 1984; Sutherland 2001). This results from the waves interacting with themselves to induce a mean flow which itself modifies the structure of the waves.

If the waves are of such large amplitude that the wave-induced mean flow exceeds the horizontal group velocity then they exhibit self-acceleration instability, meaning that the interaction eventually causes the waves to overturn and break (Sutherland 2001). At smaller but non-negligible amplitudes, the interaction modifies the structure of the amplitude envelope through weakly nonlinear dynamics. If the amplitude envelope grows in time, the waves are said to be modulationally unstable. Numerical simulations have shown that the time scale for self-acceleration is faster than parametric subharmonic instability where the amplitude envelope encompassing the wavepacket has non-negligible curvature (Sutherland 2006b). Therefore

https://doi.org/10.1017/S0022112006003016 Published online by Cambridge University Press

self-acceleration, not wave–wave interactions, should be primarily responsible for the initial weakly nonlinear-governed wavepacket modulation.

The purpose of this paper is to examine a weakly nonlinear equation that describes the evolution of these wavepackets and thereby to establish bounds on the modulational stability of the waves as they depend upon frequency, amplitude and wavepacket extent.

Weakly nonlinear equations have been derived by Grimshaw (1975) for vertical modes in a channel that are modulated horizontally and by Tabaei & Akylas (2003) for weakly viscous internal wave beams emanating from a localized oscillating object. A straightforward perturbation theory approach for horizontally periodic internal waves in uniformly stratified fluid, which is akin to that for finite-amplitude surface and interfacial internal waves (Thorpe 1968), fails. This is because monochromatic plane internal gravity waves are an exact solution of the fully nonlinear equations of motion.

Nonetheless, it is well-established that horizontally periodic internal wavepackets induce a mean flow which is analogous to the Stokes drift for surface waves. Using Hamiltonian fluid mechanics, Scinocca & Shepherd (1992) derived a formula for the pseudomomentum of internal waves. For Boussinesq waves in particular, the wave-induced mean flow (which is the pseudomomentum per unit mass) is given at leading order by

$$U(z,t) \equiv -\langle \xi \zeta \rangle, \tag{1.1}$$

in which ξ is the vertical displacement, $\zeta = \partial_z u - \partial_x w$ is the vorticity, and the angle brackets denote averaging over one horizontal wavelength.

Fully nonlinear numerical simulations have demonstrated that (1.1) accurately represents the mean horizontal motion due to waves even when the waves are close to breaking amplitude (Sutherland 2001). The mean flow is established as soon as the waves are generated, whether at a solid boundary or within the fluid by a dynamic source. Thus shear-generated waves transport momentum, as can be measured by the wave-induced mean flow associated with them (Sutherland 2006).

Fully nonlinear numerical simulations (not shown) demonstrate that waves, even if created by a moving, horizontally periodic heat source, which propagate away induce a mean flow and that in order to conserve momentum this flow is exactly compensated for by a reverse flow at the level of the source.

To model the interaction between waves and the wave-induced mean flow, equations have been derived for weakly nonlinear three-dimensional wavepackets (Shrira 1981), for finite-amplitude wavepackets (Akylas & Tabaei 2005) and wavepackets that experience the effects of weak background rotation (Akylas, private communication).

In § 2. we explicitly use (1.1) to write a weakly nonlinear equation for horizontally periodic, vertically localized internal wavepackets. The formula includes higher-order linear dispersion terms, which are shown to influence the nonlinear evolution of non-hydrostatic waves non-negligibly . After describing the numerical methods in § 3 the results of weakly nonlinear theory are compared with fully nonlinear numerical simulations in § 4. In § 5 the stability of weakly nonlinear wavepackets is assessed, and the the major results are summarized in § 6.

2. Theory

The fully nonlinear equations describing the motion of inviscid Boussinesq two-dimensional internal waves in a non-rotating environment are given in terms of total

https://doi.org/10.1017/S0022112006003016 Published online by Cambridge University Press

streamfunction, ψ_T, and total density, ρ_T, by

$$\frac{\mathrm{D}\nabla^2\psi_T}{\mathrm{D}t} = g\frac{\partial\rho_T}{\partial x} \tag{2.1}$$

and

$$\frac{\mathrm{D}\rho_T}{\mathrm{D}t} = 0. \tag{2.2}$$

The former describes how vorticity is generated by the baroclinic torque; the latter describes the conservation of mass for an incompressible fluid. In both, $\mathrm{D}/\mathrm{D}t = \partial_t + u_T\partial_x + w_T\partial_z$ is the material derivative constructed from the components of the total horizontal and vertical velocity, $u_T = -\partial_z\psi_T$ and $w_T = \partial_x\psi_T$, respectively. The associated vorticity field is $\zeta_T \equiv \partial_z u_T - \partial_x w_T = -\nabla^2\psi_T$.

The total density can be decomposed into a background density, $\bar{\rho}(z)$, and a fluctuation density, $\rho(x, z, t)$. Here we will assume the fluid is uniformly stratified so that the squared buoyancy frequency, given by $N^2 \equiv -(g/\rho_0)\mathrm{d}\bar{\rho}/\mathrm{d}z$, is constant. In this circumstance, the vertical displacement field, ξ, is proportional to the fluctuation density:

$$\xi = -\left(\frac{\mathrm{d}\bar{\rho}}{\mathrm{d}z}\right)^{-1}\rho. \tag{2.3}$$

Likewise, the total velocity field can be decomposed into the sum of a mean horizontal flow, $\bar{U}$, and the fluctuation velocity (u, w). Although in practice the background flow can be an arbitrary function of z, here we will assume there is no background horizontal flow in the absence of waves and that it is non-zero only as a result of the mean flow, U, induced by waves. That is, $\bar{U} \equiv U$, in which U is given by (1.1). Unlike the usual definition of a background flow, here U is a function not only of space but of time.

Finally, we will assume that the initial weakly nonlinear evolution involves interactions only between waves and the wave-induced mean flow.

Explicitly, we write

$$f = \mathrm{Re}\{A_f(z, t)\exp[\mathrm{i}(kx + mz - \omega t)]\} \tag{2.4}$$

in which f represents any one of the fluctuation fields, ψ, ξ, ζ, etc., and Re denotes the real part. $A_f(z, 0)$ describes the structure of the initial amplitude envelope which encompasses waves with constant wavenumber vector components k (assumed positive) and m. The fast-time evolution is assumed to be set by a constant frequency ω which is given by the dispersion relation,

$$\omega = N\frac{k}{\kappa} = N\cos\Theta, \tag{2.5}$$

in which $\kappa \equiv (k^2 + m^2)^{1/2}$. $|\Theta|$ is the angle formed by lines of constant phase with the vertical. Explicitly defining $\Theta = \tan^{-1}(m/k)$, the sign of Θ equals the sign of m.

Substituting (2.4) in (1.1) with $f \equiv \xi$ and ζ gives

$$U(z, t) = -\tfrac{1}{2}\mathrm{Re}\{A_\xi A_\zeta{}^\star\}. \tag{2.6}$$

Putting these results in (2.1) and extracting the coefficients of the $\exp[\mathrm{i}(kx+mz-\omega t)]$ terms gives

$$\{[\partial_t - \mathrm{i}(\omega - kU)][\partial_{zz} + 2\mathrm{i}m\partial_z - \kappa^2] + \mathrm{i}k\partial_{zz}U\}A_\psi = -\mathrm{i}kN^2A_\xi. \tag{2.7}$$

https://doi.org/10.1017/S0022112006003016 Published online by Cambridge University Press

Similarly, (2.2) and (2.3) combine to give

$$\{\partial_t - \mathrm{i}(\omega - kU)\}A_\xi = \mathrm{i}kA_\psi. \tag{2.8}$$

Eliminating A_ψ from these two equations gives the evolution equation for A_ξ:

$$\{[\partial_t - \mathrm{i}(\omega - kU)][\partial_{zz} + 2\mathrm{i}m\partial_z - \kappa^2] + \mathrm{i}k\partial_{zz}U\}[\partial_t - \mathrm{i}(\omega - kU)]A_\xi = k^2N^2A_\xi. \tag{2.9}$$

For infinitesimally small-amplitude waves, U is negligibly small. Assuming the vertical extent, σ, of the wavepacket is broad so that $\epsilon \equiv 1/(k\sigma) \ll 1$, standard perturbation methods (e.g. Whitham 1974) reproduce the linear Schrödinger equation. If the maximum vertical displacement, A_0, is so large that $\alpha \equiv kA_0$ is of order ϵ, then perturbation theory at next order reveals that this equation is modified through the addition of a term which represents the Doppler-shifting of the waves by the wave-induced mean flow. In a frame of reference moving with the vertical group speed $c = -(N/k)\cos^2\Theta\sin\Theta$, the resulting equation for A_ξ is

$$\partial_t A_\xi = \mathrm{i}\tfrac{1}{2}c_m\partial_{ZZ}A_\xi + \tfrac{1}{6}c_{mm}\partial_{ZZZ}A_\xi - \mathrm{i}kUA_\xi. \tag{2.10}$$

Here $c_m = -(N/k^2)\cos^3\Theta(1 - 3\sin^2\Theta)$ and $c_{mm} = 3(N/k^3)\cos^4\Theta\sin\Theta(3 - 5\sin^2\Theta)$ are the second and third partial derivatives, respectively, of ω with respect to m, and $Z \equiv z - ct$ denotes the moving vertical coordinate.

Equation (2.10) includes the third-order Z-derivative term, which results from including the next-order ϵ terms in the perturbation expansion. This accounts for the dispersion of waves having frequency $\omega \simeq \omega_c \equiv N(2/3)^{1/2}$, for which $c_m = 0$.

The corresponding equation for vorticity has the form of (2.10) but with ξ replaced by ζ. Together with (1.1), this forms a closed coupled system of equations for ξ and ζ. However, the symmetry of the equations implies that if initially $A_\zeta = \mathscr{C}A_\xi$ for some constant $\mathscr{C}$, then this proportionality relationship holds for all time. This is confirmed by explicit numerical solutions of the coupled equations.

Linear theory gives the leading-order approximation to the proportionality constant: $\mathscr{C} = -N\kappa$. Thus $U = N\kappa|A|^2/2$ and the weakly nonlinear evolution of a horizontally periodic, vertically localized internal wavepacket is represented well by a single differential equation in one variable:

$$A_t = \mathrm{i}\tfrac{1}{2}c_m A_{ZZ} + \tfrac{1}{6}c_{mm}A_{ZZZ} - \mathrm{i}\tfrac{1}{2}Nk^2\sec\Theta|A|^2A. \tag{2.11}$$

Here, for notational convenience, we have defined $A \equiv A_\xi$ and denoted partial derivatives by subscripts.

Weakly nonlinear vertically localized, horizontally-periodic internal waves are therefore governed by a nonlinear Schrödinger equation in which the nonlinear term has a pure imaginary coefficient and the linear dispersive terms can be positive or negative depending upon the value of Θ. Neglecting the A_{ZZZ} term in (2.11), the resulting equation is a special case of the formulae derived by Akylas & Tabaei (2005).

3. Numerical methods

In what follows, we compare the numerically integrated solutions of the weakly nonlinear equation (2.11) with the results of fully nonlinear numerical simulations. In practice, the length and time scales are set by assigning $k = 1$ and $N = 1$, although the results here will be presented explicitly in terms of k and N or, where convenient, of the corresponding horizontal wavelength λ_x and buoyancy period T_B.

https://doi.org/10.1017/S0022112006003016 Published online by Cambridge University Press

m/k	Θ (deg.)	ω/N	$\frac{k}{N}c$	$\frac{k^2}{N}c_m$	$\frac{k^3}{N}c_{mm}$	$\frac{k}{N}\frac{1}{\alpha^2}U_0$
−0.4	−21.8	0.92	0.32	−0.469	−1.91	0.54
−0.7	−35.0	0.82	0.38	−0.007	−1.05	0.61
−1.4	−54.5	0.58	0.27	0.194	0.09	0.86

TABLE 1. Parameters and weakly nonlinear equation coefficients used for the simulations presented here.

We focus upon the evolution of Gaussian wavepackets with vertical displacement field given initially by

$$\xi(x, z, 0) = A(z, 0)\cos(kx + mz) \qquad \text{with} \qquad A(z, 0) = A_0 \mathrm{e}^{-z^2/2\sigma^2}. \tag{3.1}$$

We take $\epsilon \equiv 1/(k\sigma) = 0.1$ throughout and the internal wavepacket evolution is determined as it depends upon $\alpha \equiv kA_0$ and the relative vertical wavenumber m/k. The parameters for the featured simulations are given in table 1. These are chosen to illustrate the dependence of the qualitative difference between the evolution of small- and large-amplitude wavepackets upon the wave frequency, whether it be below, near, or above the critical frequency, ω_c, of waves having the largest vertical group speed. The amplitudes examined are as large as $\alpha = 0.3$ ($A_0 \simeq 0.048\lambda_x$), which is close to the amplitude at which the waves are prone to breaking due to self-acceleration (Sutherland 2001).

The initial wave-induced mean flow is

$$U(z, 0) = U_0 \mathrm{e}^{-z^2/\sigma^2} \qquad \text{with} \qquad U_0 = \frac{1}{2}\frac{N}{k}\alpha^2 \sec\Theta. \tag{3.2}$$

It is possible to correct A iteratively for the initial effects of Doppler-shifting by the background flow. However, this is not done here because the change is negligibly small even for α as large as 0.3.

Centred finite differencing is used to compute derivatives in (2.11), and the field is advanced in time using the leapfrog method with an Euler backstep taken every 20 steps to avoid splitting errors. Typical runs are performed on a horizontally periodic domain having free-slip upper and lower boundary conditions, spanning $|Z| \leqslant 102.4k^{-1}$ with a resolution of $0.4k^{-1}$. Fields are advanced in time by $0.001N^{-1}$ up to $t = 150N^{-1}$ (about 24 buoyancy periods). Doubling the resolution makes a negligible difference to the results.

The fully nonlinear numerical simulation solves (2.1) and (2.2) with an additional Laplacian diffusion term added to the right-hand side of each equation, as has been described by Sutherland (2006). This is necessary to ensure numerical stability, but the corresponding Reynolds and Schmidt numbers based on the horizontal wavenumber and buoyancy frequency are set to be large enough that diffusion plays a negligible role over the duration of the simulations. The calculations are performed in a stationary, (z, t), frame of reference, and the output is transformed to (Z, t) variables through the translation $Z = z - ct$.

4. Results

First the results of fully nonlinear numerical simulations are presented. Figure 1 shows the evolution of a small- and large-amplitude wavepacket with $m = -0.4k$.

https://doi.org/10.1017/S0022112006003016 Published online by Cambridge University Press

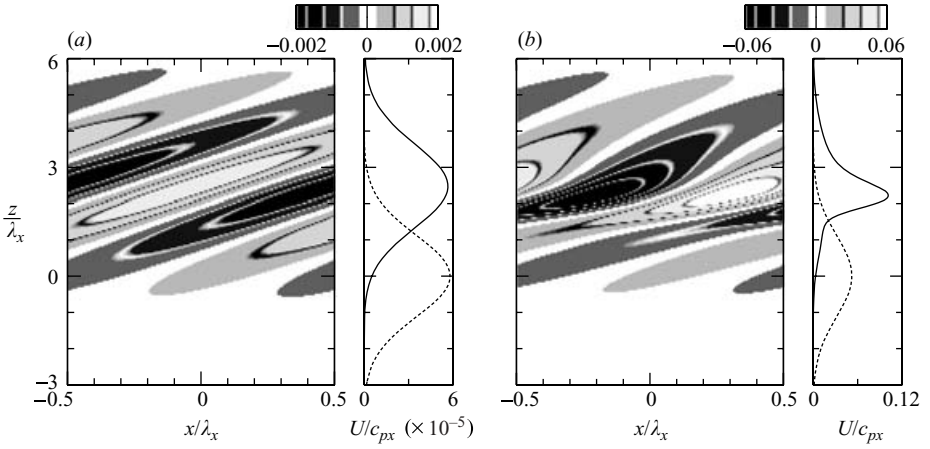


FIGURE 1. Results of fully nonlinear numerical simulation of a wavepacket given initially by (3.1) with $\epsilon^{-1} \equiv k\sigma = 10$, $m = -0.4k$ and (*a*) $\alpha = 0.01$ and (*b*) $\alpha = 0.3$. In both cases the left panel shows greyscale contours of the normalized vertical displacement field ξ/λ_x at time $t = 50N^{-1}$ and the right panel plots U relative to the predicted horizontal phase speed $c_{px} = \omega/k$ at this time (solid line) and at time $t = 0$ (dashed line).

The small-amplitude wavepacket (figure 1*a*), which is initially centred about $z = 0$, propagates upwards at a nearly constant speed equal to the vertical group speed. At time $t = 50N^{-1}$ it is centred about $z = ct \simeq 16k^{-1} \simeq 2.5\lambda_x$. Comparing the initial and final profiles of U, the wavepacket amplitude is found to decrease moderately while its extent broadens, as anticipated from linear theory.

The late-time structure of the large-amplitude wavepacket, shown in figure 1(*b*), is qualitatively different. Rather than broadening, the wavepacket decreases in vertical extent and the amplitude increases. The fine structure also becomes more complex with constant-phase lines tilting closer to the vertical near the vertical midpoint of the wavepacket.

By comparison with figure 1(*b*), figure 2(*a*) shows that the weakly nonlinear equations are able to capture the essential features of the fully nonlinear evolution at this time. The greyscale image shows normalized contours of $\xi(x, z, 50N^{-1})$, which are computed from the amplitude envelope through the relationship (2.4) with $f \equiv \xi$. Likewise, the wave-induced mean flow is plotted against $z = Z + ct$.

Figures 2(*b*) and 2(*c*) show the corresponding plots at time $t = 50N^{-1}$ of the real and imaginary parts of A and of its magnitude, $|A|$, respectively. These are plotted against Z instead of z and so represent the structure of the wavepacket in a frame of reference moving with the vertical group speed. The fact that the peak amplitude lies moderately below $Z = 0$ is an indication that weakly nonlinear effects decelerate the progress of the wavepacket in this instance.

The fully nonlinear evolution over time of the wavepacket breadth and amplitude is represented by time series of $U(Z, t)$ in six simulations, as shown in figure 3. In each case, the correlation $-\langle \xi\zeta \rangle$ is computed at successive times and each result in translated from z to $Z = z - ct$ coordinates.

In the three simulations of small-amplitude wavepackets, shown in figure 3(*a–c*), the flow is peaked along $Z = 0$ for all time, confirming that these wavepackets move upward at the vertical group speed predicted by linear theory. The simulation with

https://doi.org/10.1017/S0022112006003016 Published online by Cambridge University Press

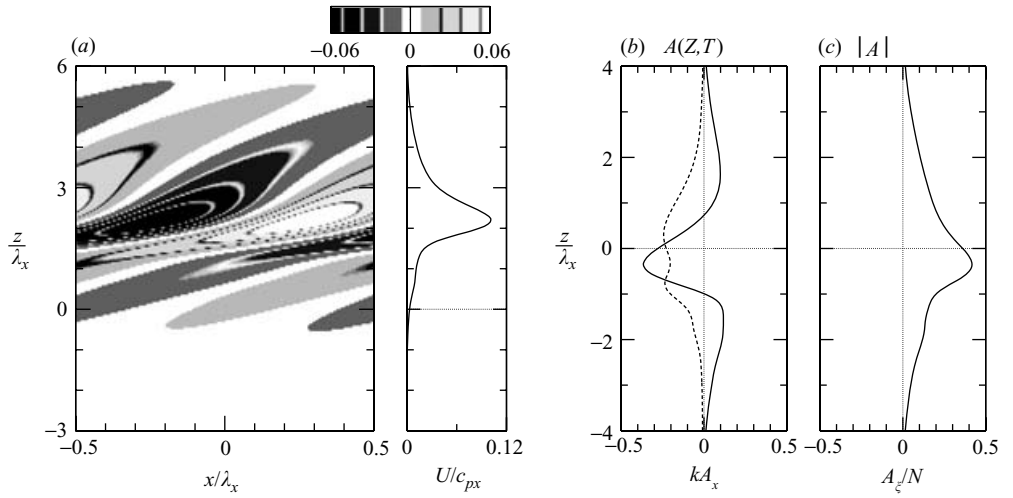


FIGURE 2. Solution of weakly nonlinear equations corresponding to simulation shown in figure 1(*b*). (*a*) Greyscale contours of the normalized vertical displacement field ξ/λ_x at time $t = 50N^{-1}$ and plot of U relative to the predicted horizontal phase speed $c_{px} = \omega/k$ at this time. The remaining panels show the real (solid line) and imaginary (dashed line) parts of (*b*) $kA(Z,T)$ and (*c*) $k|A(Z,T)|$ taken at $T = t = 50N^{-1}$ and with $Z = z - ct$.

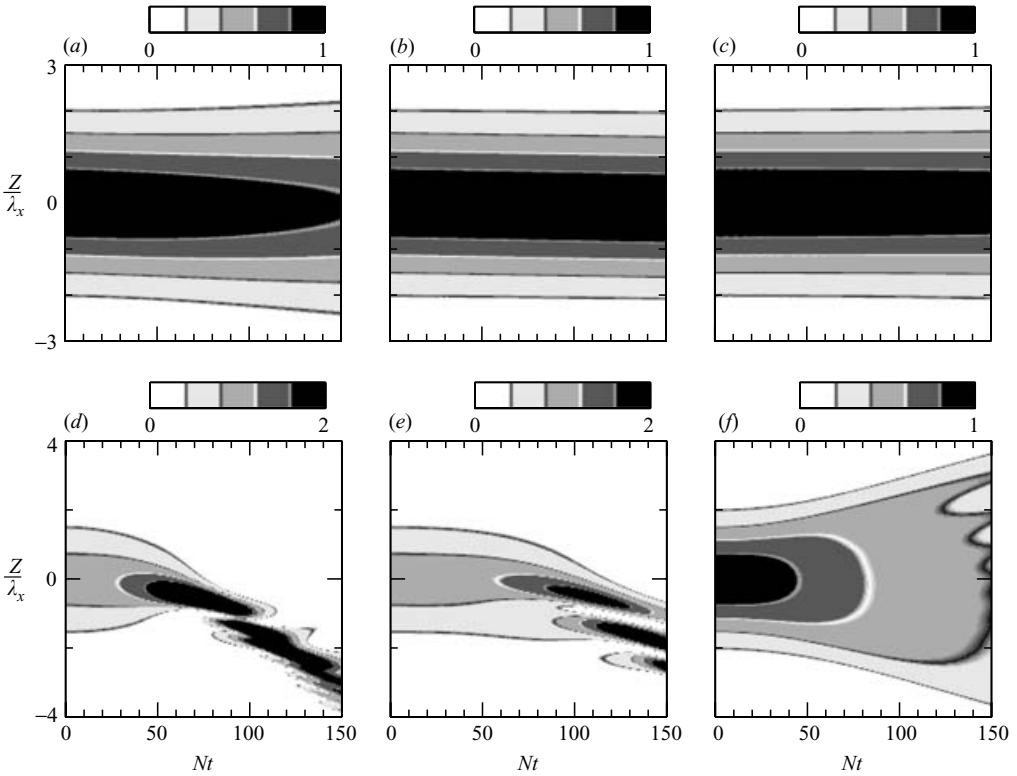


FIGURE 3. Time series of normalized wave-induced mean flow $U(Z,t)/U_0$ in fully nonlinear numerical simulations with $\alpha = 0.01$ and (*a*) $m = -0.4k$, (*b*) $m = -0.7k$, (*c*) $m = -1.4k$ and with $\alpha = 0.30$ and (*d*) $m = -0.4k$, (*e*) $m = -0.7k$, f) $m = -1.4k$.

https://doi.org/10.1017/S0022112006003016 Published online by Cambridge University Press

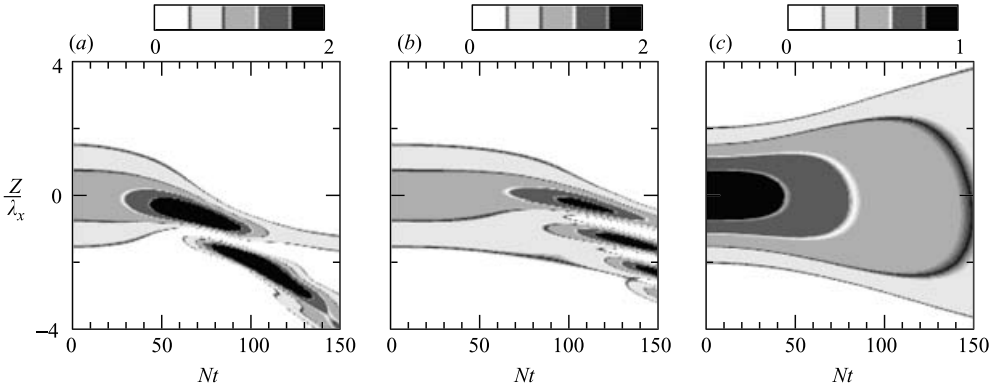


FIGURE 4. As in figure 3(*d–f*), but for U/U_0 computed from the weakly nonlinear equation.

$m=-0.4k$ exhibits the most dispersion through the broadening and decrease in peak amplitude of the wavepacket.

The behaviour of the corresponding large-amplitude wavepackets is qualitatively different. In simulations with $\alpha=0.3$ and $m=-0.4k$ (figure 3*d*) and $m=-0.7k$ (figure 3*e*) the maximum value of the wave-induced mean flow more than doubles whereas in the simulation with $m=-1.4k$ (figure 3*f*) the maximum value drops by more than half due to nonlinearly enhanced dispersion. Another notable feature of the large-amplitude simulations with $m=-0.4k$ and $-0.7k$ is the deceleration of the wavepacket relative to the vertical group speed. In particular, the peak value of U moves downward at a relative rate of $-0.25N/k$ whose magnitude is comparable with c.

These qualitative, and most of these quantitative, features are captured by the corresponding solutions of the weakly nonlinear equation (2.11). As expected, the linear dispersion of the wavepacket is represented well in the solution computed for small-amplitude wavepackets (not shown). Comparing figures 4(*a–c*) with figures 3(*d–f*), respectively, the weakly nonlinear equations are found to represent well the nonlinearly enhanced broadening of the wavepacket with $m=-1.4k$ and the amplitude growth, envelope narrowing and vertical deceleration of wavepackets with $m=-0.4k$ and $-0.7k$. Discrepancies appear at late times because subharmonic wave excitation, which results in fine vertical-scale structures, is not captured by (2.11).

Test studies (not shown) demonstrate that all three terms on the right-hand side of (2.11) are necessary to capture the evolution of non-hydrostatic internal waves. Because the wavepacket evolves so that it narrows, the third-order Z-derivative term eventually approaches the same order as the second-order Z-derivative term. The asymmetry introduced by the third-order derivatives is ultimately what is responsible for the vertical deceleration of the wavepacket as a whole. These observations are quantified in the next section.

5. Analysis

To gain further insight into the behaviour of the weakly nonlinear solutions we examine the initial temporal evolution of the amplitude envelope through its effect upon the wave-induced mean flow. Assuming that A is real-valued initially gives

$$\partial_t U|_{t=0} = \tfrac{1}{6} N k c_{mm} \sec\Theta A A_{ZZZ}. \tag{5.1}$$

Because the coefficients of the A_{ZZ} and the nonlinear terms are pure-imaginary, they do not affect the first-order time-derivative. Equation (5.1) predicts that the

https://doi.org/10.1017/S0022112006003016 Published online by Cambridge University Press

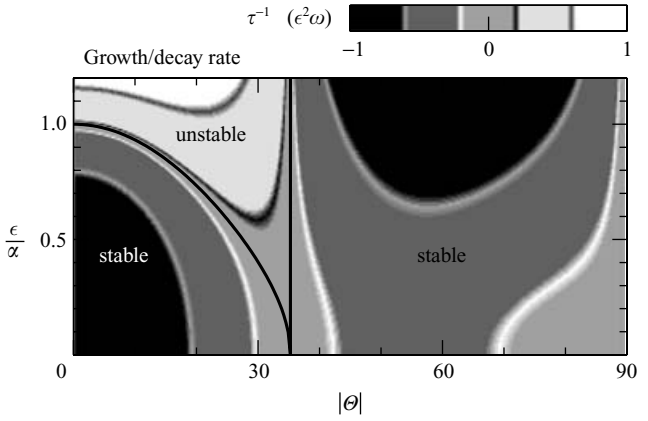


FIGURE 5. Solid lines delineate stability regimes for a Gaussian wavepacket as they depend upon the relative wave frequency, measured by $\Theta = \cos^{-1}(\omega/N)$, and the relative amplitude, measured by $\alpha/\epsilon = A_0\sigma k^2$. Greyscale contours show the normalized inverse time scale associated with the growth ($\tau^{-1} > 0$) or decay ($\tau^{-1} < 0$) of the amplitude envelope.

amplitude of a Gaussian wavepacket grows on the trailing flank of the wavepacket if $|\Theta| < \sin^{-1}(3/5)^{1/2} \simeq 50.8^\circ$. Otherwise the amplitude grows on the leading flank. Hence the symmetry-breaking evident in figures 4(a, b) is less evident in the small-amplitude simulations.

If c_m is non-zero, the early evolution of large-amplitude wavepackets is determined primarily by the second-order time-derivative

$$U_{tt}|_{t=0} = \tfrac{1}{2}Nk\sec\Theta\{c_m kA(2U_Z A_Z + U_{ZZ}A) + \tfrac{1}{2}{c_m}^2\left({A_{ZZ}}^2 - AA_{ZZZZ}\right) + \tfrac{1}{18}{c_{mm}}^2\left({A_{ZZZ}}^2 + AA_{ZZZZZZ}\right)\}. \quad (5.2)$$

Thus linear dispersive effects, manifested through non-zero values of c_m and c_{mm}, are necessary for U to change in time, even in the nonlinear regime.

At the centre of a Gaussian wavepacket

$$U_{tt}|_{t=0,Z=0} = -\frac{1}{2}\frac{N^3}{k}\alpha^2\epsilon^2\left\{\frac{k^2c_m}{N}\sec\Theta\left(\alpha^2 + \frac{k^2c_m}{N}\epsilon^2\right) + \frac{k^6{c_{mm}}^2}{N^2}\sec\Theta\epsilon^4\right\}. \quad (5.3)$$

This is negative for all α and ϵ if c_m is positive; that is, if $|\Theta| > \sin^{-1}(3^{-1/2}) \simeq 35.3^\circ$. So wavepackets that have frequency smaller than the frequency of waves with the fastest vertical group speed are modulationally stable: nonlinear effects accentuate the rate at which the amplitude decreases in time.

Now suppose $|\Theta| < \sin^{-1}(3^{-1/2})$. Assuming the wavepacket is so broad that the last term in the braces on the right-hand side of (5.3) can be neglected, then U_{tt} is negative only if $\alpha^2 + (k^2c_m/N)\epsilon^2$ is negative. Explicitly, the stability boundary is

$$\frac{\alpha}{\epsilon} = \sqrt{\cos^3\Theta(1 - 3\sin^2\Theta)}, \quad (5.4)$$

as can be determined from standard modulation theory for the nonlinear Schrödinger equation. This curve is plotted and modulational stability regimes are indicated in figure 5. This figure also indicates growth and decay rates through the time scale τ,

https://doi.org/10.1017/S0022112006003016 Published online by Cambridge University Press

which is defined by

$$\tau \equiv \mathrm{sgn}(U_{tt})\sqrt{|U/U_{tt}|}\Big|_{t=0,Z=0}. \tag{5.5}$$

A surprising result is that internal waves propagating with the maximum vertical group speed are modulationally unstable due to weakly nonlinear effects even if $\alpha/\epsilon \ll 1$. In dimensional units, this is the condition $A_0 \ll 1/(k^2\sigma)$.

6. Conclusions

We have shown that the early time evolution of a horizontally periodic, vertically compact wavepacket is represented well by accounting only for interactions between the waves and the wave-induced mean flow. The resulting weakly nonlinear equation predicts that waves with frequencies between $\simeq 0.82N$ and N are unstable in the sense that the amplitude envelope grows where the curvature is large and it advances vertically at a slower rate. Large-amplitude waves with smaller frequency disperse rapidly due to weakly nonlinear effects. Although fully nonlinear wavepackets eventually break down due to parametric subharmonic instability, the simulations presented here show that the weakly nonlinear equation accurately depicts the wavepacket evolution beyond 15 buoyancy periods, which reasonably represents the life cycle of large-amplitude non-hydrostatic waves in the atmosphere and ocean.

This work arose from discussions with T. Akylas, G. Carnevale and B. Young. The research was supported by the Canadian Foundation for Climate and Atmospheric Science (CFCAS).

REFERENCES

Akylas, T. R. & Tabaei, A. 2005 Resonant self-acceleration and instability of nonlinear internal gravity wavetrains. In *Frontiers of Nonlinear Physics* (ed. A. Litvak), pp. 129–135. Institute of Applied Physics.

Benielli, D. & Sommeria, J. 1996 Excitation of internal waves and stratified turbulence by parametric instability. *Dyn. Atmos. Oceans* **23**, 335–343.

Fritts, D. C. & Dunkerton, T. J. 1984 A quasi-linear study of gravity-wave saturation and self-acceleration. *J. Atmos. Sci.* **41**, 3272–3289.

Grimshaw, R. H. J. 1975 Nonlinear internal gravity waves and their interaction with the mean wind. *J. Atmos. Sci.* **32**, 1779–1793.

Klostermeyer, J. 1991 Two- and three-dimensional parametric instabilities in finite amplitude internal gravity waves. *Geophys. Astrophys. Fluid Dyn.* **64**, 1–25.

Koudella, C. R. & Staquet, C. 2006 Instability mechanisms of a two-dimensional progressive internal gravity wave. *J. Fluid Mech.* **548**, 165–196.

Lombard, P. N. & Riley, J. J. 1996 On the breakdown into turbulence of propagating internal waves. *Dyn. Atmos. Oceans* **23**, 345–355.

Scinocca, J. F. & Shepherd, T. G. 1992 Nonlinear wave-activity conservation laws and Hamiltonian structure for the two-dimensional anelastic equations. *J. Atmos. Sci.* **49**, 5–27.

Shrira, V. I. 1981 On the propagation of a three-dimensional packet of weakly non-linear internal gravity waves. *Intl J. Non-Linear Mech.* **16**, 129–138.

Sutherland, B. R. 2001 Finite-amplitude internal wavepacket dispersion and breaking. *J. Fluid Mech.* **429**, 343–380.

Sutherland, B. R. 2006*a* Rayleigh wave-internal wave coupling and internal wave generation above a model jet stream. *J. Atmos. Sci.* **63**, 1042–1055.

Sutherland, B. R. 2006*b* Internal wave instability: Wave-wave vs wave-induced mean flow interactions. *Phys. Fluids.* **18**, Art. No. 074107.

Tabaei, A. & Akylas, T. R. 2003 Nonlinear internal gravity wave beams. *J. Fluid Mech.* **482**, 141–161.

Thorpe, S. A. 1968 On the shape of progressive internal waves. *Phil. Trans. R. Soc. Lond.* A **263**, 563–614.

Whitham, G. B. 1974 *Linear and Nonlinear Waves*. John Wiley and Sons.

https://doi.org/10.1017/S0022112006003016 Published online by Cambridge University Press